ACS OMEGA

http://pubs.acs.org/journal/acsodf

Article

Prediction of Sinter Properties Using a Hyper-Parameter-Tuned Artificial Neural Network

Soumya Sahoo, Ashutosh Pare, Subhabrata Mishra, Shatrughan Soren,* and Surendra Kumar Biswal

Cite This: *ACS Omega* 2023, 8, 11782−11789

Read Online

ACCESS | Metrics & More | Article Recommendations

ABSTRACT: The present work aims at performing prediction validation for the physical properties of coke layered and nonlayered hybrid pelletized sinter (HPS) using artificial neural networks (ANNs). Physical property analyses were experimentally performed on the two HPS products. The ANN model was then trained to obtain the best prediction results with the grid-search hyper-parameter tuning method. The learning rate, momentum constant, and the number of neurons varied over specified ranges. The binary variable conversion was utilized to assess the two sintering processes. The nonlayered HPS product of 4 mm micropellets at basicity 1.75 and using 8% coke shows a good combination of physical properties, whereas HPS of 4 mm micropellets at 1.5 basicity using 4% coke as fuel and 2% coke as layering gives a radical improvement in physical properties. The yield of the HPS product is 96.07%, with the shatter index (SI), tumbler index (TI), and abrasion index (AI) values being 86.12, 79.60, and 5.74%, respectively. Hence, HPS can be preferred by implementing the layering of coke powder. The prediction analyses showed that the multilayer perceptron model (MLP) network with a 4-29-5 structure showed prediction accuracies of over 99.99% and a mean squared error (MSE) of 2.87×10^{-4}. It verifies the accuracy and prediction effectiveness of the hyper-parameter-tuned ANN model.

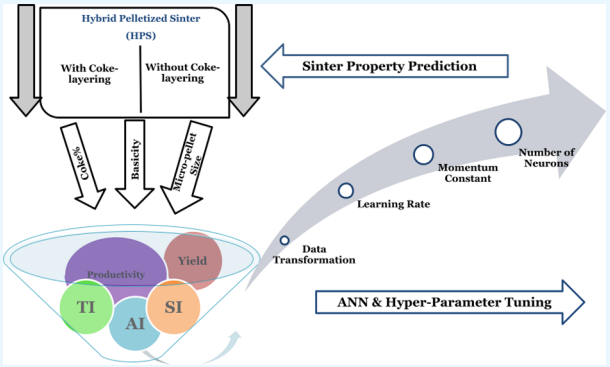

1. INTRODUCTION

Iron ore is the most valuable, finite, and nonrenewable resource for iron and steel making. High reaction efficiency and enhanced heat transfer characteristics make the blast furnace (BF) promising for modern iron production. There is a growing tendency in the production of steel as iron and steel are widely used in modern civilization. The growing tendency has led to the depletion of high-quality iron ore resources and the agglomeration processes to achieve a homogeneous material's size that could ensure a suitable operation in the furnace. There are five iron ore agglomeration technologies such as briquetting, nodulization, extrusion, pelletization, and sintering. However, sinter and pellets are two dominant blast furnace burdens. Indian iron ores are friable in nature, and this leads to the generation of fines during various stages of mining. These fines were of no use and usually get exported at very fewer values because of their unsuitability for blast furnace operations until sintering came into the scenario. Utilization of fines in the blast furnace reduces surface porosity. However, these fines are rich in minerals and utilization of fines is the need of hour.

Iron ore, coke, sinter, and limestone are the primary raw materials required to be fed into the blast furnace. Sintering can be considered as a traditional thermal agglomeration technique. Sinter is used as a feed material of the blast furnace to enhance productivity and reduce fuel consumption. For a successful sintering process, a mixture of iron ore (−10 mm + 100 μ), return fines, coke breeze, flux (limestone, dolomite, olivine, serpentine, etc.), and moisture is mixed uniformly and charged at the top of sinter strand. The feed sample is ignited to a higher temperature of around 1200−1300 °C and the blower attached at the bottom of the bed sucks the combustion front, thus letting the hot air to roast the feed material and pass through the sinter bed. The sintering process produces iron ore agglomeration of size 10−40 mm with better reducibility values than lumps. Utilization of a higher proportion of quality agglomerates in the burden increases the productivity of the blast furnace. The sintering process increases the productivity and reduces the requirement of fuel, flux, and operation time.

Iron ore of Indian origin shows a typical characterization result. These iron-bearing minerals are generally soft and friable due to the presence of ochreous goethite.[1] A bulk

Received: September 15, 2022
Accepted: March 9, 2023
Published: March 21, 2023

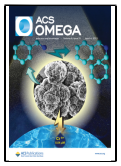

amount of fines is generated over time, mostly during the classification of ores through crushing, grinding, screening, and beneficiation processes. Even though a part of these generated high-grade fines is used directly in the existing agglomeration process as a feed material, most of its low and medium-grade ores remain unused. Upgradation of the Fe value through the beneficiation route is needed. The fine concentrate is generated as the liberation of iron phase minerals is at finer sizes. It can be used as a feed material for making pellets through the pelletization route.

In general, the pelletization of iron ore is a process where the feed is a mixture of high-grade hematite/magnetite ore mixed with a binder, coke breeze, and limestone as additives to form green pellets. Then, pellets are indurated at high temperatures to maintain requisite metallurgical properties for producing iron and steel. The heat-hardening process of pelletization is an energy-intensive process.[2] The sintering process is an alternative to using the fine concentrate through the hybrid-pellet sintering process to maintain bed permeability by reducing the overall energy consumption of making iron and steel.[3] Effective utilization of low and lean-grade iron ore fines is a critical issue from both environmental and economic points of view.

The hybrid pelletized sintering (HPS) process comes into the frontline to overcome these problems and maximize the utilization of iron ore fines. To utilize the iron ore fines in plants, Nippon Kokan Keihin company (presently, JFE Steel Corporation) developed the HPS process.[4] Investigators have tried to improve the utilization of iron ore fines in sinter beds by making HPS.[5,6] The HPS process is a modified form of the conventional sintering process. In this HPS process, iron ore fines are pelletized to produce micro pellets. Green micro-pellets are then layered with coke powder before being charged into the sinter strand. Sinter pot tests have confirmed the benefits of the preferential addition of coke onto the surface of the green balls and the superior properties of the final agglomerates produced using the HPS process.[7] In this process, the return fines act as the nucleus, and lime acts as the agglomerating agent. The HPS process allows the maximal use of iron ore fines with no loss of productivity. Hence, compared to the conventional sintering process, the HPS process can produce lower SiO_2 sinter of good strength due to the formation of solid diffusion bonding during sintering.[3]

Implementing the sintering technique in blast furnaces came into existence because of its uniqueness in obtaining a product with a desirable composition to be used as a burden material for the BF. Moreover, as an essential input parameter in blast furnaces, the stable chemical composition of the sintered product.[8] Preference is given to the iron content (Fe), alumina (Al_2O_3), calcium (CaO), and magnesium (MgO) and the amount of basicity, while studying the chemical composition of the sintered product.[9−12] Sinters need to have high cold strength (commonly defined by the tumbler index (TI)), low reduction degradation index (RDI), and high reducibility index (RI).[8] Iron ore sinters' structure and characteristics mainly depend on the chemistry of the raw material fed into the sinter pot, the size distribution of every particle, and the process parameters like the percentage and size of the coke required, the portion of the addition of the return fines and maintaining basicity. Reports suggest that having 0.212−3.35 mm coke size gives a stable, homogenous, and regular blast furnace operation.[13,14] Another vital parameter that needs to be focused on during the experiment is the sinter bed's permeability. It has been conveyed that we get an adequately packed sinter bed for a size range of 3−6 mm micropellets.[15]

Laitinen and Saxén[16] noted that understanding the relationship between the composition of bedding pile, quality of sinter, and plant performance is a highly complex study, and to date, no suitable mathematical and statistical models have been developed to describe these interdependent relations accurately. Zhang et al.[17] confirmed that multi-objective optimization is necessary for better understanding of the sintering process and its parameters. Specific parameters like the complex systems of quality, cost, energy consumption, and output must be mathematically correlated under transient states with the corresponding emphasis on production.

Shigaki and Narazaki[18] presented a multi-layered neural network using a machine learning approach. The operational rules were optimized for the sintering process in the iron and steel-making plant to obtain the products meeting the given quality specifications. Song et al.[19] developed a neural network-based machine learning algorithm to predict the sinter quality. The analysis was performed on the data collected from various sources. The drum index and screening index were studied via cluster analysis. The prediction accuracy of the classification and regression models was observed to have good generalization ability, and accurate sinter quality indices were realized. Shao et al.[20] noted the strong input−output relation in the sintering process parameters. The characteristic nonlinearity and considerable time delays in the overall sintering processes upon variations with process parameters led to the development of neural network models with high prediction accuracy and more vital self-learning ability. Er et al.[21] performed a prediction analysis for the quality of chemical components in finished sinter minerals. The input and output data were correlated using hybrid fuzzy neural networks (FNN) and genetic algorithms (GA). The backpropagation algorithm was employed in online operations to improve system precision. The results demonstrated excellent prediction performance and accuracy of the system. Wang et al.[22] employed back propagation neural networks for cost predictions in actual sintering productions. The process employed conjugate gradient algorithms with an inexact line search route on the generalized curry principle. Prediction accuracies of over 94% were observed.

The above-discussed models were developed for single sintering processes and focused on limited quality indices. The variations in the sintering process parameters significantly affect the physicochemical properties of sintered products, as well as the associated yields and productivity. Optimizing and validating these processes can immediately prove beneficial for industrial productivity, cost, energy benefits, and the quality of sinter ores. The present ANN-based study correlates two sintering processes (conventional sintering and HPS) in a unified model. In varying percentages, the layered and nonlayered samples were tested for sinter development with varying basicity and micropellet sizes. The exact yield, productivity, SI, TI, and AI were analyzed to distinguish the effects of variations in sinter input parameters. The ANN model employs hyperparameter tuning to predict and validate resultant physical properties accurately. The consequent predicted values are studied via statistical techniques and plot presentations.

https://doi.org/10.1021/acsomega.2c05980
ACS Omega 2023, 8, 11782−11789

2. MATERIALS AND METHODS

2.1. Materials. Iron ore having a Fe content of 60.46% and a size fraction −10 mm was collected from a mine in the Barbil region, Keonjhar, Odisha. Scrubbing followed by beneficiation was carried out to improve the Fe (T) to 62.47%. The scrubbing study of the said sample was reported in an earlier published article by Sahoo et al.[1] Coke breeze was used as solid fuel and limestone as a flux for this sintering experiment. The proximate analysis of the coke breeze used in the sintering experiment is shown below in Table 1. The as-received coke breeze was crushed and screened to obtain a −4 + 3 mm size. The limestone was crushed and ground to 100 μm.

Table 1. Proximate and Ultimate Analysis of Coke Breeze

fixed carbon, %	moisture, %	ash, %	volatile matter, %
85.71	2.7	8.42	3.16

2.2. Experimental HPS Process. During the size reduction and beneficiation process, iron ore fines were generated. These iron ore fines were appropriately mixed and considered for pelletization in a disc pelletizer (1 m diameter). Different micropellets (1−5 mm) were produced to be used as a feed material in the sinter pot for the HPS process. A laboratory-scale sinter pot (25 kg) was used to carry out the sintering experiments, where the experiments were done in batch mode. Two sets of experiments were carried out to study the improvement in sinter characteristics. The first sets of experiments were carried out using micropellets without coke layering called NL-HPS (Nonlayered: NL), and the second set of experiments with coke powder layering called L-HPS (Layered: L). Besides, the micropellet coating was done at the end of the pelletization process by adding 2% of coke powder to the disc pelletizer. However, the total coke percentage in both sets of experiments was identical. For a broader range of HPS-related experiments, parameters like the coke %, size of micropellets, and basicity percentage are given in Table 2. The schematic diagram depicting the sintering process is shown in Figure 1. The sinter mechanical properties like SI, TI, AI, and metallurgical properties like RI and RDI were tested for each experiment to generate the datasheet for ANN modeling.

2.3. ANN Approach. The existence of multiple sintering processes and a more extensive set of parametric variations leads to the development of a complex and less accurate correlation for predicting the input requirements as per production needs. These problems are recently being addressed using ANNs. The ANNs are an interconnected set of artificial neurons to mathematically correlate the input set of variables to their corresponding outputs. The networks possess self-learning capability via algorithms, enabling them to produce optimized results. It is primarily achieved via backpropagation analysis, where the errors are evaluated at each step to perfect the prediction outputs.

3. RESULTS AND DISCUSSION

The physical properties of all sets of sinters from the two groups of the experiment by varying the size of micropellets (1, 2, 3, 4, and 5) were carried out, and it was noted that 4 mm micropellet size improved yield and productivity with relatively higher SI and TI values and lower AI values. Tables 3 and 4 represent the best set of results. From all stages of data generated using without layering of coke, it is observed from

Table 2. Different Parametric Studies for Coke-Coated and Uncoated Micro-Pellets Based on HPS Experiments[a]

experiment code	details of the experiment	
	coke %	basicity
without coke powder layering		
A_{0i3}	2	1.5
B_{0i3}	4	1.5
C_{0i3}	6	1.5
D_{0i3}	8	1.5
E_{0i3}	2	1.75
F_{0i3}	4	1.75
G_{0i3}	6	1.75
H_{0i3}	8	1.75
I_{0i3}	2	2
J_{0i3}	4	2
K_{0i3}	6	2
L_{0i3}	8	2
2% coke powder layering		
A_{i3}	0	1.5
B_{i3}	2	1.5
C_{i3}	4	1.5
D_{i3}	6	1.5
E_{i3}	0	1.75
F_{i3}	2	1.75
G_{i3}	4	1.75
H_{i3}	6	1.75
I_{i3}	0	2
J_{i3}	2	2
K_{i3}	4	2
L_{i3}	6	2

[a] *i* denotes the micropellet size of 1, 2, 3, 4, and 5 mm. 1 mm refers to −2 + 1 mm and so for other sizes of micropellets.

Table 3 that L_{043} gives the best physical properties. As presented in Table 3, to conduct the L_{043} experiment, 8% coke and 2% basicity were used. Table 4 shows the physical properties of data generated using 2% coke layering on the micro-pellet size of 4 mm. It is perceptible that H_{43} gives the best result for physical properties, considering 6% coke and 1.75% basicity. There is a minor variation in the physical properties of G_{43} and H_{43}. From Table 4, it is seen that G_{43} requires 4% coke and 1.5% as basicity. As the consumption of both coke and limestone is comparatively less in G_{43} than in H_{43}, G_{43} is preferable. Comparing all data sets from Tables 3 and 4 shows the necessity of coke layering on micropellets to get results with higher yield and productivity, better SI and TI, and low AI.

3.1. ANN Model Development. The qualitative and quantitative evaluation techniques in the sintering processes are discussed in the previous sections. The experimental limitations of repetition and optimization occur via resource availability, process cost, and testing. This limits the validation of the performance parameters via standard statistical techniques. An ANN simulates the biological nervous system structure to model nonlinear relationships and develop data prediction methods. This is achieved by similar learning and training methods to correlate the input and target variables. In the present work, a unified ANN model is developed and tuned by performing analysis over a range of hyperparameters, viz., the learning rate, the momentum constant, and the number of neurons.[23] The grid search-based hyper-parameter tuning method was employed in the present model. The

https://doi.org/10.1021/acsomega.2c05980
ACS Omega 2023, 8, 11782−11789

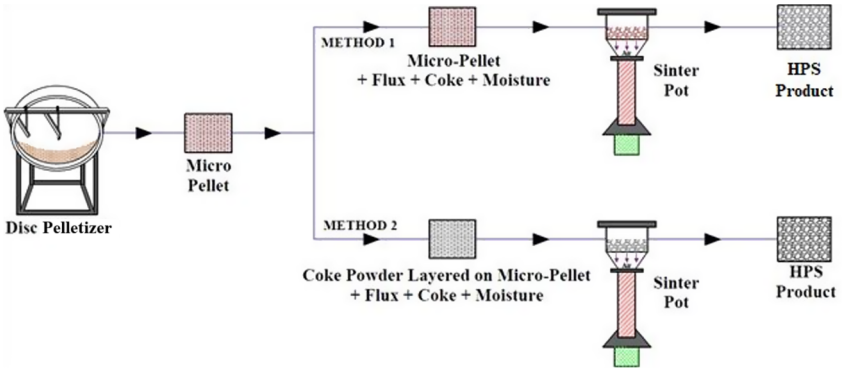

Figure 1. Process flowsheet for the HPS process.

Table 3. Physical Properties of NL-HPS Sintered Products

sinter code	yield, %	productivity, $t/(m^2\ d)$	SI, %	TI, %	AI, %
A_{043}	47.30	36.50	37.48	36.23	8.50
B_{043}	57.19	44.13	50.02	49.38	8.49
C_{043}	62.01	47.85	55.05	53.39	7.05
D_{043}	64.92	50.09	58.20	57.61	5.53
E_{043}	48.84	37.68	43.09	42.26	8.41
F_{043}	60.76	46.88	63.29	62.90	8.02
G_{043}	68.50	52.85	70.00	69.37	6.40
H_{043}	71.00	54.78	70.58	69.80	5.30
I_{043}	48.05	37.08	44.16	43.05	8.20
J_{043}	60.33	46.55	65.29	63.60	8.12
K_{043}	68.93	53.19	69.02	68.97	7.10
L_{043}	71.43	55.12	70.23	69.00	5.52

Table 4. Physical Properties of L-HPS Sintered Products

sinter code	yield, %	productivity, $t/(m^2\ d)$	SI, %	TI, %	AI, %
A_{43}	20.00	15.43	53.61	43.82	12.03
B_{43}	75.20	58.02	73.61	63.82	10.03
C_{43}	98.26	72.54	86.06	79.04	5.80
D_{43}	98.31	73.00	86.85	80.27	5.01
E_{43}	22.74	17.51	53.63	43.93	11.57
F_{43}	76.49	58.95	73.50	63.93	9.57
G_{43}	96.07	72.07	86.12	79.60	5.74
H_{43}	98.39	73.01	86.00	79.85	5.32
I_{43}	22.80	17.59	53.84	44.05	11.53
J_{43}	76.93	59.35	73.84	64.05	9.60
K_{43}	96.00	72.00	80.00	79.50	5.74
L_{43}	98.00	72.19	86.17	79.30	5.77

method uses the brute force approach to explore every possible combination of hyper-parameters in the model to estimate model performance and then select the best possible performance combinations. The coke %, basicity, and micro-pellet size are input parameters. The output parameters are yield percentage, productivity, SI, TI, and AI. Besides, Beskardes et al.[24] opted a similar procedure for the RDI estimation of the sinter via correlating multiple input and output parameters. The best model performance is obtained by the least mean squared error values (eq 1).[25]

$$\mathrm{MSE} = \frac{\left[\sum (X_{\mathrm{Exp}} - X_{\mathrm{ANN}})^2\right]}{n} \tag{1}$$

The neural network hyper-parameters are deterministic variables defining the network structure for training, learning, prediction fitting, and obtaining the best possible overall minima/maxima. The number of layers in the neural network is noted to improve the accuracy of the network. The direct correlation between the input and output layer is often reported to cause network under-fitting. It is resolved by adding a hidden layer(s) with varying numbers of neurons. The addition of multiple hidden layers might improve the model's accuracy. The parallel consequence of the same exists in the form of significantly larger training times and a higher probability of over-fitting validation curves. The learning rates in the neural networks control the weight variation factors for prediction optimizations. The lower learning rates cautiously increase weights, leading to higher precision, but with more significant analysis times.

Similarly, higher learning rates lead to nonconvergence of the solution, as no optima may occur due to higher losses and overshooting ranges. The momentum constants are added to the neural networks to increase weights over previous iterations, which speeds up the learning rates and simultaneously assists in overcoming the local minima of the prediction topologies via overshooting against minor opposing gradients. The neurons determine the learning behavior of the neural networks.

Figure 2 represents the flowchart adopted for data prediction model development using the ANN. The statistical analysis and hyper-parameter tuning methodologies are accounted for using the workflow method presented above. The input and output data sets are normalized between −1 and 1 using eq 2.[26] This plays significance in evaluating the dataset on a common scale as opposed to varying orders of values found in experimental techniques. The layered and nonlayered surfaces are presented as input parameters using the data transformation technique to perform simultaneous assessment for both experimental methodologies. This is enabled by giving the value '1' and '0' for prioritizing and limiting, respectively, the methods during the training of the ANN model (Table 5).

$$Y_i = \frac{2X_i - X_{\max} - X_{\min}}{X_{\max} - X_{\min}} \tag{2}$$

The dataset matrix obtained after normalization and data transformation is then divided into training, validation, and testing subsets with a ratio of 70, 15, and 15%, respectively. The 120 points data set is analyzed from the experiments performed at the research facility at CSIR-IMMT, Bhubaneswar, Odisha, India. The Levenberg−Marquardt (LM) back-propagation algorithm has been selected as the training algorithm for the present model that employs the Gauss−Newton and gradient descent techniques for updating the

https://doi.org/10.1021/acsomega.2c05980
ACS Omega 2023, 8, 11782−11789

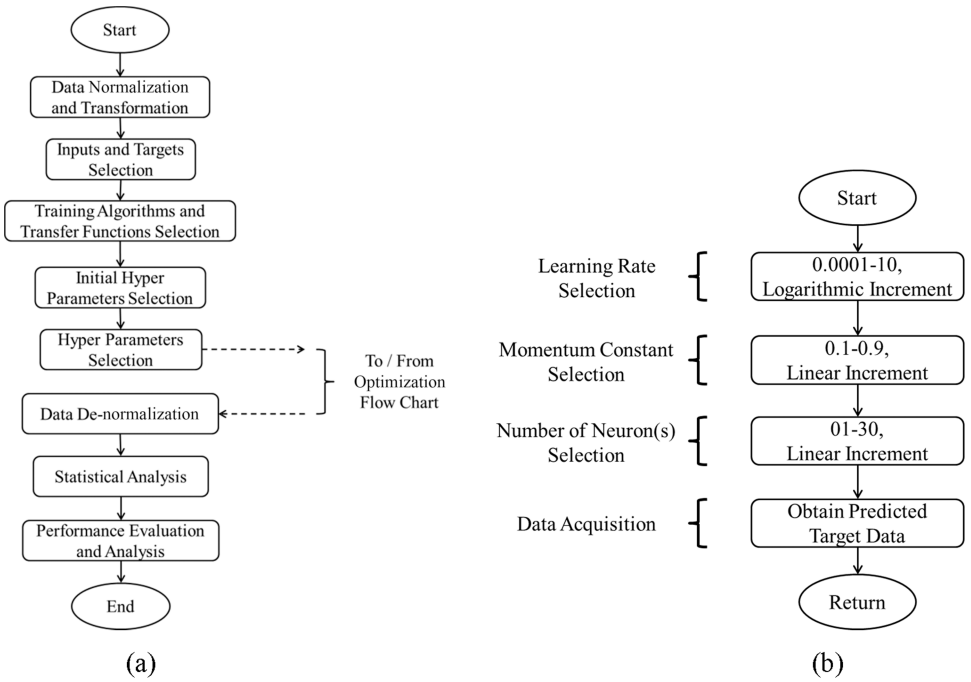

Figure 2. ANN flowchart (a) model development and (b) hyper-parameter optimization.

Table 5. Binary Variable Conversion

	layered	nonlayered
layered	1	0
nonlayered	0	1

solutions after each iteration by minimizing the damping factor and smoothening the solution to optimal values. The gradient descent with momentum (LEARNGDM) learning function, tangent sigmoid (TANSIG) (eq 3), and linear activation (PURELIN) (eq 4) transfer functions are employed in the present work. This enables the update of weights and biases by backpropagation while simultaneously calculating multiple nonlinear regressions at high speeds. The transfer functions allow the communicating medium between the neural layers.[27] The learngdm function updates the weights using eq 5, where,

$$\text{Tansig}(x) = \frac{2}{1 + \exp(-2x)} - 1 \tag{3}$$

$$\text{Purelin}(x) = x \tag{4}$$

$$dw_i = mc \times dw_{i-1} + (1 - mc) \times lr \times w_r \tag{5}$$

The present work used a multilayer perceptron model (MLP) using a single hidden layer with a varying number of neurons (1 to 30) to correlate input−output nonlinearity. The learning rates varied logarithmically from 0.0001 to 10. The momentum constants are linearly increased in the range of 0.1 to 0.9. The momentum constants update weights utilizing the history of gradient descent. The low and high momentum and learning rates values lead to variations in analysis duration and insensitiveness to the local stochastic gradients. The neural layers carry out the mathematical operation under the transfer function with suitable weights and biases. This is described using eq 6, where weight (w), bias (b), activation function (f), input (x), and output (y) are employed in mathematical evaluations. The individual neuron in the layers of the network takes the target value with a weighted sum and suitable bias. This operation is then followed by mathematical evaluation via

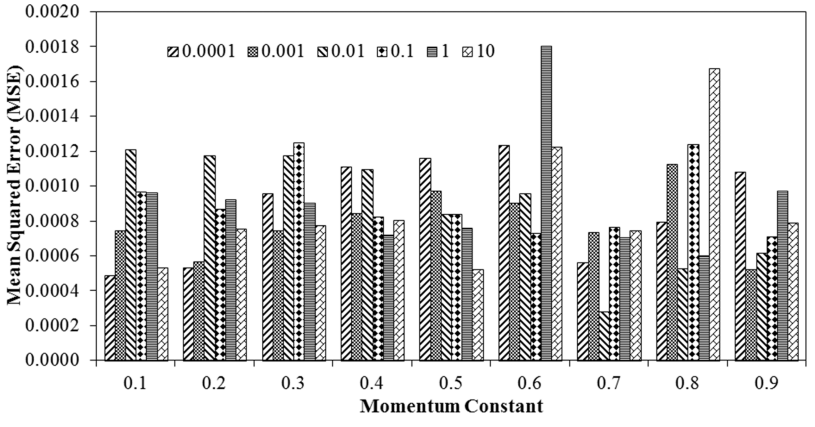

Figure 3. Variation of least MSEs with varying learning rates and constant momentum hyper-parameters.

https://doi.org/10.1021/acsomega.2c05980
ACS Omega 2023, 8, 11782−11789

Table 6. Performance Statistics of the ANN Model for Varying Numbers of Neurons at a Constant Learning Rate at Momentum Constant

learning rate	momentum constant	number of neurons in the hidden layer	MSE training	MSE testing	MSE validation
0.01	0.7	1	8.12×10^{-2}	9.55×10^{-3}	8.98×10^{-3}
0.01	0.7	2	3.31×10^{-2}	4.52×10^{-3}	4.07×10^{-3}
0.01	0.7	3	2.83×10^{-2}	4.05×10^{-3}	3.96×10^{-3}
0.01	0.7	4	1.90×10^{-2}	1.60×10^{-3}	2.39×10^{-3}
0.01	0.7	5	2.27×10^{-2}	2.39×10^{-3}	3.60×10^{-3}
0.01	0.7	6	1.69×10^{-2}	1.66×10^{-3}	1.71×10^{-3}
0.01	0.7	7	1.13×10^{-2}	2.36×10^{-3}	1.77×10^{-3}
0.01	0.7	8	5.97×10^{-3}	1.04×10^{-3}	1.75×10^{-3}
0.01	0.7	9	5.71×10^{-3}	1.23×10^{-3}	1.02×10^{-3}
0.01	0.7	10	9.04×10^{-3}	1.91×10^{-3}	2.05×10^{-3}
0.01	0.7	11	6.10×10^{-3}	7.19×10^{-4}	1.20×10^{-3}
0.01	0.7	12	1.29×10^{-2}	2.96×10^{-3}	1.99×10^{-3}
0.01	0.7	13	4.58×10^{-3}	1.29×10^{-3}	1.31×10^{-3}
0.01	0.7	14	2.26×10^{-3}	3.57×10^{-3}	2.72×10^{-3}
0.01	0.7	15	2.97×10^{-3}	1.08×10^{-3}	1.51×10^{-3}
0.01	0.7	16	2.78×10^{-3}	1.96×10^{-3}	1.70×10^{-3}
0.01	0.7	17	2.00×10^{-3}	1.15×10^{-3}	7.59×10^{-4}
0.01	0.7	18	3.74×10^{-3}	1.13×10^{-3}	1.17×10^{-3}
0.01	0.7	19	2.98×10^{-3}	1.12×10^{-3}	1.76×10^{-3}
0.01	0.7	20	3.30×10^{-3}	1.86×10^{-3}	1.64×10^{-3}
0.01	0.7	21	3.69×10^{-3}	1.95×10^{-3}	2.72×10^{-3}
0.01	0.7	22	5.59×10^{-3}	2.96×10^{-3}	2.36×10^{-3}
0.01	0.7	23	3.97×10^{-3}	1.26×10^{-3}	1.62×10^{-3}
0.01	0.7	24	6.86×10^{-4}	1.33×10^{-3}	2.66×10^{-3}
0.01	0.7	25	1.26×10^{-3}	2.25×10^{-3}	1.58×10^{-3}
0.01	0.7	26	7.14×10^{-4}	1.46×10^{-3}	8.80×10^{-4}
0.01	0.7	27	7.29×10^{-4}	1.10×10^{-3}	1.35×10^{-3}
0.01	0.7	28	9.42×10^{-4}	2.99×10^{-3}	2.06×10^{-3}
0.01	0.7	29	2.78×10^{-4}	1.06×10^{-3}	1.22×10^{-3}
0.01	0.7	30	5.56×10^{-4}	1.42×10^{-3}	2.65×10^{-3}

the convenient activation function for feeding to the next layer of mathematical operations.

$$y_j = f\left(\sum_{i=1}^{n} w_{j,i}x_i + b_j\right) \tag{6}$$

After analysis using various models, the predicted dataset is then de-normalized and statistically analyzed. The least mean squared errors are noted for each model. The best model is then selected and evaluated using parameters viz. mean squared errors, regression coefficients, and mean absolute percentage errors.

3.2. ANN Model Performance. As mentioned in the previous section, the unified ANN model was trained using the range of hyper-parameters. The least MSE values were selected for each momentum constant and learning rate set under a varying number of neurons, as shown in Figure 3. The lower MSE value was observed for varying learning rates at 0.7 momenta constant value. The least MSE was obtained at a 0.01 learning rate.

Table 6 shows the variation of MSE values of training, testing, and validation data sets for a varying number of neurons at 0.7 momenta constant and 0.01 learning rate. As mentioned above, Figure 4 shows the variation in MSEs with varying numbers of neurons under momentum and learning rate hyper-parameters. The present analysis noted the least MSEs at 29 neuron combinations.

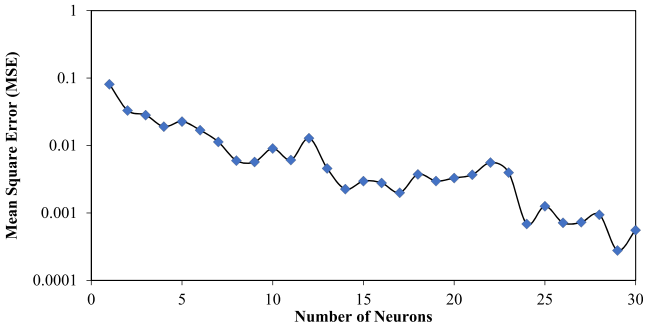

Figure 4. Variation of the MSEs with the number of neurons at a constant learning rate and momentum constant.

Figures 5 and 6 show the parity plots for experimental physical properties against the predicted physical properties for the sintered processes employed in the present work. The ANN predicted values were compared against the experimental values after de-normalization. The predicted values were noted to be the best fit within ±1% of the experimental data set. This nature was observed for physical property analysis after the previously discussed sinter processes. The extended statistical analysis showed an MSE of 0.000278 and regression coefficient (eq 7) values above 0.999, representing that the predicted data set is in excellent agreement with the experimental output dataset. It also assures the reliability of the designed neural network model obtained via the hyper-parameter tuning methodology.

https://doi.org/10.1021/acsomega.2c05980
ACS Omega 2023, 8, 11782−11789

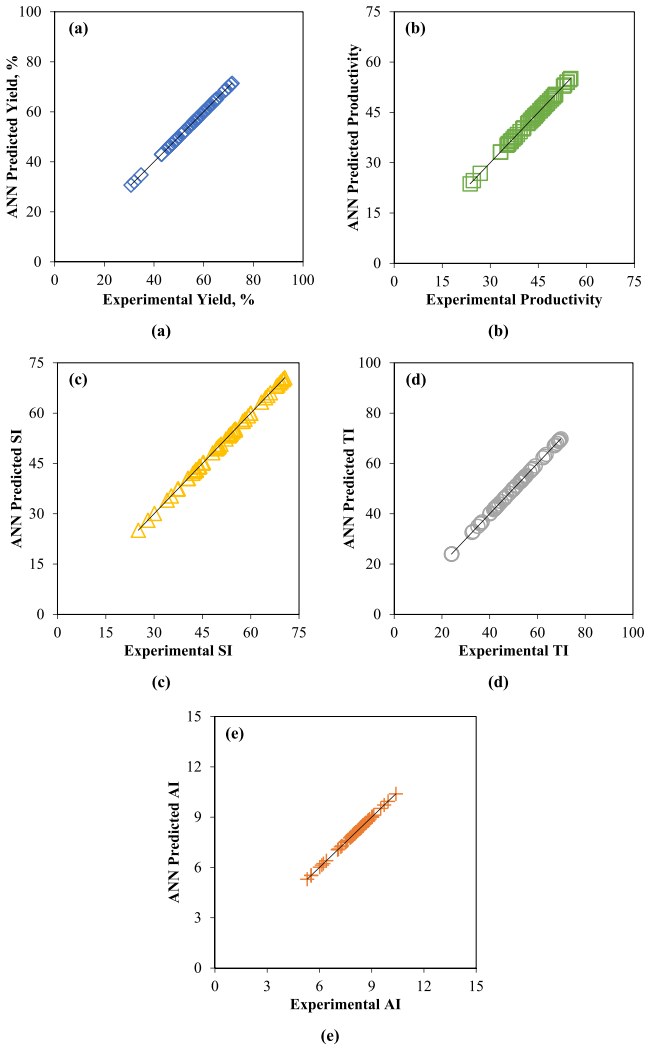

Figure 5. Comparison of experimental and ANN predicted physical properties for NL-HPS.

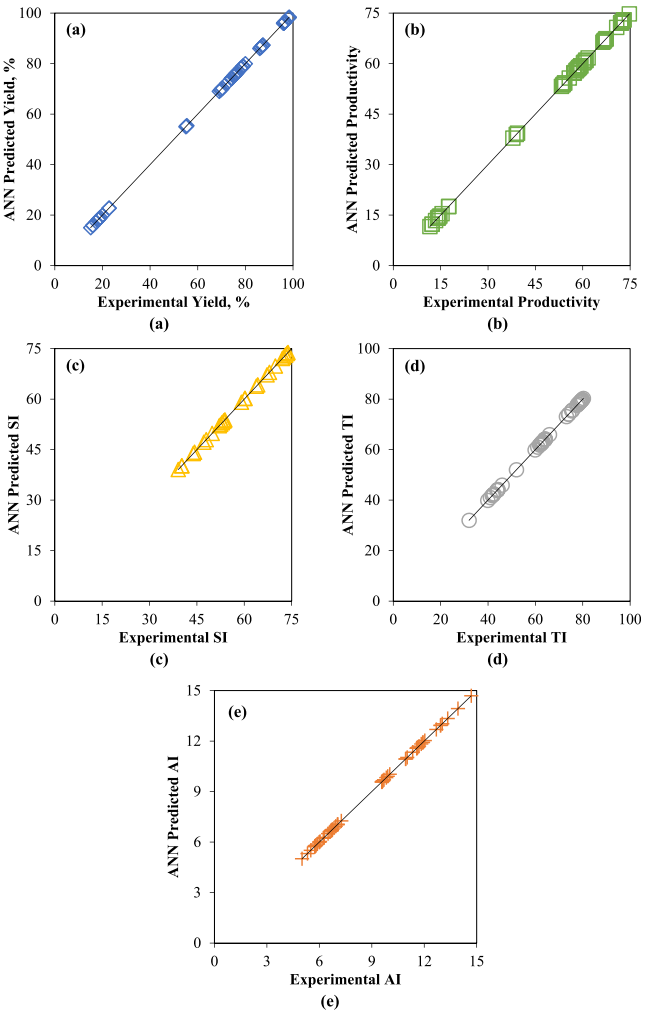

Figure 6. Comparison of experimental and ANN predicted physical properties for L-HPS.

$$R = \sqrt{\left[1 - \left\{\frac{\sum_{i=1}^{n}(X_{\mathrm{Exp}} - X_{\mathrm{ANN}})^2}{\sum_{i=1}^{n} X_{\mathrm{ANN}}^2}\right\}\right]} \quad (7)$$

4. CONCLUSIONS

The experimental study was performed on iron ore sinters to develop hybrid pelletized sinter and conventional sinters. The yield, productivity, and physical property analyses were performed for varying basicity, micropellet sizes, and coke percentages. The experiments generated by coke powder layering and without the coke powder layering process conclude that the hybrid pelletized sintering process with coke layering (L-HPS) is efficient; it is a nonconventional sintering process taking into account future trends in iron ore resources aiming radical improvements in yield, productivity, and physical properties of iron ore sinter. The most significant outcomes witnessed from this study are enlisted below.

(i) It was confirmed that at 1.5% basicity, using 4% coke as fuel and 2% coke powder layering gives the desired yield of 96.07%, having SI, TI, and AI values as 86.12, 79.60, and 5.74%, respectively. HPS can be treated as an environmentally sustainable process as we can utilize iron ore fines and consume less coke, which is the need of the hour.

(ii) The hyper-parameter-tuned ANN model showed a prediction accuracy of over 99% and an MSE of 2.78 $\times$ 10^{-4}. It offers the high accuracy of the proposed prediction model. The developed network structure and proposed hyper-parameters set the bench work for sintering quality prediction for two independent processes that can further prove helpful in optimizing the metallurgical properties of the sinter based on the proposed input parameters.

(iii) The developed ANN modeling work can be extended for the plant scale, where the sinter plant data can be used for better accuracy.

AUTHOR INFORMATION

Corresponding Author

Shatrughan Soren − *Indian Institute of Technology (Indian School of Mines), Dhanbad 826004, India;* orcid.org/0000-0002-5984-0042; Email: ssoren24@gmail.com, ssoren@iitism.ac.in

Authors

Soumya Sahoo − *Indian Institute of Technology (Indian School of Mines), Dhanbad 826004, India*

https://doi.org/10.1021/acsomega.2c05980
ACS Omega 2023, 8, 11782−11789

Ashutosh Pare − *Indian Institute of Technology (Indian School of Mines), Dhanbad 826004, India*
Subhabrata Mishra − *CSIR-Institute of Minerals and Materials Technology, Bhubaneswar 751013, India; Academy of Scientific and Innovative Research (AcSIR), Ghaziabad 201002, India*
Surendra Kumar Biswal − *Tirupati Graphene and Mintech Research Centre, Bhubaneswar 751029, India*

Complete contact information is available at: https://pubs.acs.org/10.1021/acsomega.2c05980

Author Contributions

S.S.: Conceptualization, investigation, writing original draft, and reviewing. A.P.: Investigation, writing original draft, and editing. S.M.: Setup development, investigation, and editing. S.S.: Supervision and reviewing. S.K.B.: Supervison.

Notes

The authors declare no competing financial interest.
The raw/processed data required to reproduce these findings cannot be shared as the data also form part of an ongoing study.

■ ACKNOWLEDGMENTS

The authors thank Dr. Prabhas Chandra Beuria (Senior Principal Scientist, CSIR-IMMT, Bhubaneswar, India) for his extended support, including designing, developing, and fabricating the Sinter facility and carrying out the experimental work. They also acknowledge the help of Er. Sachida Nanda Sahu (Principal Scientist, CSIR-IMMT, Bhubaneswar, India) for his continuous support during the experiment. The authors also extend their regards to the Head of the Mineral Processing Department and the Director, CSIR-IMMT, Bhubaneswar, for permission to conduct this research work.

■ REFERENCES

(1) Sahoo, S.; Sahu, S. N.; Sahoo, R. K.; Soren, S.; Biswal, S. K. A Study on Removal of Clay Minerals from Barbil Region Iron Ore; Effect of Scrubbing Followed by Pelletization. *Min. Metall. Explor.* **2021**, *38*, 105−116.
(2) Sahu, S. N.; Baskey, P. K.; Barma, S. D.; Sahoo, S.; Meikap, B. C.; Biswal, S. K. Pelletization of Synthesized Magnetite Concentrate Obtained by Magnetization Roasting of Indian Low-Grade BHQ Iron Ore. *Powder Technol.* **2020**, *374*, 190.
(3) Mousa, E. A.; Babich, A.; Senk, D. A Novel Approach for Utilization of Ultra-Fines Iron Ore in Sintering Process. *Steel Res. Int.* **2015**, *86*, 1350−1360.
(4) Fernández-González, D.; Piñuela-Noval, J.; Verdeja, L. F. Iron Ore Agglomeration Technologies. In *Iron Ores and Iron Oxide Materials*; IntechOpen, 2018.
(5) Pal, J.; Ghorai, S.; Goswami, M. C.; Prakash, S.; Venugopalan, T. Development of Pellet-Sinter Composite Agglomerate for Blast Furnace. *ISIJ Int.* **2014**, *54*, 620.
(6) Komatsu, O.; Noda, H. Commercial Production of Iron Ore Agglomerates Using Sinter Feeds Containing a Large Amount of Fine Ores. *ISIJ Int.* **1993**, *33*, 454.
(7) Sakamoto, N.; Noda, H.; Iwata, Y.; Saito, H.; Miyashita, T. Fundamental Investigation On Production Conditions Of New Iron Ore Agglomerates For Blast Furnace Burdens And Evaluation Of Their Properties. *Tetsu-to-Hagane* **1987**, *73*, 1504−1511.
(8) Fernández-González, D.; Ruiz-Bustinza, I.; Mochón, J.; González-Gasca, C.; Verdeja, L. F. Iron Ore Sintering: Raw Materials and Granulation. *Miner. Process. Extr. Metall. Rev.* **2017**, *38*, 36−46.
(9) Bristow, N. J.; Engloo, C. Sintering Properties of Iron Ore Mixes Containing Titanium. *ISIJ Int.* **1992**, *32*, 819.
(10) Lu, L.; Holmes, R. J.; Manuel, J. R. Effects of Alumina on Sintering Performance of Hematite Iron Ores. *ISIJ Int.* **2007**, *47*, 349−358.
(11) Zhang, G.; Wu, S.; Chen, S.; Zhu, J.; Fan, J.; Su, B. Optimization of Dolomite Usage in Iron Ore Sintering Process. *ISIJ Int.* **2013**, *53*, 1515.
(12) Higuchi, K.; Takamoto, Y.; Orimoto, T.; Sato, T.; Koizumi, F.; Shinagawa, K.; Furuta, H. Quality Improvement of Sintered Ore in Relation to Blast Furnace Operation. *Nippon Steel Tech. Rep.* **2006**, *94*.
(13) Dezfuly, N. T. P.; Moghadam, A. H. Effect of Coke Particle Size on Sinter Quality. In *Materials Science and Technology Conference and Exhibition 2011, MS and T'11*; 2011; *2*.
(14) Plant, S.; Versions, C. Sinter Plant, Technical Session-2: Depleting Iron Ore Reserves - Maximising Sintering & Pelletizing Usage. In *International Seminar on Start-up and Stand up India from Mines to Steel*; Mecon Ltd., Ed.; Ranchi, 2016; 1−5.
(15) Roshan, V.; Kumar, K.; Kumar, R.; Nageswara Rao, G. V. S. Preparation of Iron Ore Micro-Pellets and Their Effect on Sinter Bed Permeability. *Trans. Indian Inst. Met.* **2018**, *71*, 2157.
(16) Laitinen, P. J.; Saxén, H. A Neural Network Based Model of Sinter Quality and Sinter Plant Performance Indices. *Ironmaking Steelmaking* **2007**, *34*, 109.
(17) Zhang, J. H.; Xie, A. G.; Shen, F. M. Multi-Objective Optimization and Analysis Model of Sintering Process Based on BP Neural Network. *J. Iron Steel Res. Int.* **2007**, *14*, 1−5.
(18) Shigaki, I.; Narazaki, H. A Machine-Learning Approach for a Sintering Process Using a Neural Network. *Prod. Plan. Control* **1999**, *10*, 727.
(19) Song, L.; Qing, L.; Xiaojie, L.; Yanqin, S. Synthetically Predicting the Quality Index of Sinter Using Machine Learning Model. *Ironmaking Steelmaking* **2020**, *47*, 828.
(20) Shao, H.; Yi, Z.; Chen, Z.; Zhou, Z.; Deng, Z. Application of Artificial Neural Networks for Prediction of Sinter Quality Based on Process Parameters Control. *Trans. Inst. Meas. Control* **2020**, *42*, 422.
(21) Er, M. J.; Liao, J.; Lin, J. Fuzzy Neural Networks-Based Quality Prediction System for Sintering Process. *IEEE Trans. Fuzzy Syst.* **2000**, *8*, 314−324.
(22) Wang, B.; Yang, B.; Sheng, J.; Chen, M.; He, G. An Improved Neural Network Algorithm and Its Application in Sinter Cost Prediction. In *Proceedings - 2009 2nd International Workshop on Knowledge Discovery and Data Mining, WKKD 2009*; 2009.
(23) Kumar, V.; Pare, A.; Tiwari, A. K.; Ghosh, S. K. Efficacy Evaluation of Oxide-MWCNT Water Hybrid Nanofluids: An Experimental and Artificial Neural Network Approach. *Colloids Surf. A Physicochem. Eng. Asp.* **2021**, *620*, No. 126562.
(24) Beskardes, A.; Hames, Y.; Cevik, S.; Kaya, K.; Ozdemir, E. Fuzzy Logic Based Sinter RDI Optimization. In *Proceedings - 2019 4th International Conference on Power Electronics and their Applications, ICPEA 2019*; 2019.
(25) Pare, A.; Ghosh, S. K. A Unique Thermal Conductivity Model (ANN) for Nanofluid Based on Experimental Study. *Powder Technol.* **2021**, *377*, 429.
(26) Pare, A.; Ghosh, S. K. Surface Qualitative Analysis and ANN Modelling for Pool Boiling Heat Transfer Using Al2O3-Water Based Nanofluids. *Colloids Surf. A Physicochem. Eng. Asp.* **2021**, *610*, No. 125926.
(27) Kumar, V.; Sairam, S. D. S. S.; Kumar, S.; Singh, A.; Nayak, D.; Sah, R.; Mahapatra, P. C. Prediction of Iron Ore Sinter Properties Using Statistical Technique. *Trans. Indian Inst. Met.* **2017**, *70*, 1661.